PCCP

PAPER

View Article Online
View Journal | View Issue

Cite this: *Phys. Chem. Chem. Phys.*, 2014, **16**, 23355

Nanoscale phononic interconnects in THz frequencies†

Aris P. Sgouros,[ab] Mahesh R. Neupane,[c] M. M. Sigalas,*[a] N. Aravantinos-Zafiris[a] and Roger K. Lake[c]

Received 27th May 2014,
Accepted 18th September 2014

DOI: 10.1039/c4cp02328e

www.rsc.org/pccp

Phononic computing is emerging as an alternative computing paradigm to the conventional electronic and optical computing. In this study, we propose and analyze various phononic interconnects, such as nano-scaled phononic resonators, waveguides and switches, on the ⟨111⟩ surface of 3C-SiC and 3C-GeSi with substitutional and vacancy defects. This is achieved by simultaneously introducing defects of various types, and by varying their specific locations on the surface. To calculate the intrinsic and the defect-induced vibrational properties, such as the phononic bandgap and the variation in the phonon spectra, the total phonon density of states (TPDOS) and the partial phonon density of states (PPDOS) were calculated using molecular dynamics simulations with semi-empirical potentials. The proposed phononic interconnects, in conjunction with electronic and/or photonic interconnects, can be used in the current and future devices.

I. Introduction

Phononics or phonon engineering involves the control and manipulation of phonon interactions and transport.[1] With the advent of naturally occurring two-dimensional (2D) van der Waals materials such as graphene, transition metal dichalcogenides (TMDC) and artificially made 2D materials, this field of engineering is becoming a very interesting research area with applications ranging from the macroscale to the nanoscale.[2] Although research utilizing engineered materials and their heterostructures in this field of engineering started as early as 1992,[3,4] it is only recently that there has been intense effort to analyze and manipulate phonons at the nanoscale in order to design nanodevices operating at terahertz (THz) frequencies. In analogy with the corresponding electronic and photonic devices, there are studies of thermal diodes and rectification,[5–8] thermal memory[9] and charge density wave transistors.[10,11] With the realization of these types of devices, phononic computing will appear as an alternative computing paradigm to the conventional electronic and optical computing, increasing our ability to manipulate and store information in the nanoscale.

Parallel to phononic device research, there is an effort to manipulate phonons and the thermal conductivity[12,13] for improved thermoelectric properties. The materials studied in those studies are carbon based such as carbon nanotubes, graphene, and graphene composites.[12–14] Several studies with silicon based materials[15–18] have also shown that, due to the confinement-induced changes, the phonons and lattice thermal conductivity are significantly modified in nanoscale systems, such as silicon membranes,[16] two dimensional phononic crystals,[15–17] and silicon surfaces with silicon posts.[18]

Electronic and optical interconnect design tradeoffs are well researched and understood.[19] However, to realize and integrate the phononic devices with the existing conventional device architectures, phononic interconnect components such as waveguides, resonators, and switches are needed. In this study, we propose and analyze various phononic interconnect components, such as nano-scaled phononic resonators, waveguides and switches, realized on ⟨111⟩ surfaces of group IV elements, such as 3C-SiC and 3C-GeSi (the surfaces with the highest density) by introducing defects on the surface of these materials. These materials are widely used in the optoelectronics devices.[20–25] The growth of ordered systems with alternating atoms, similar to the SiC and GeSi systems, are commonly achieved using advanced deposition techniques such as molecular beam epitaxy (MBE),[26] atomic layer deposition (ALD),[27] self-assembly[28] and chemical vapor deposition (CVD).[29]

The appearance of phononic band gaps (PBG) is very important for the creation of localized states around the defects and these materials are expected to have wide PBG.[30,31] The defects are introduced either by removing (vacancy defects) or by replacing atoms (substitutional defects). The removal and placement of individual atoms and lines of atoms in Si has been demonstrated.[25,32,33] The process of defect introduction leads to the generation of strongly localized vibrational modes around the

[a] *Department of Materials Science, University of Patras, 26504 Patras, Greece. E-mail: sigalas@upatras.gr*
[b] *School of Chemical Engineering, National Technical University of Athens (NTUA), 15780 Athens, Greece*
[c] *Laboratory for Terascale and Terahertz Electronics (LATTE), Department of Electrical, And Computer Engineering, University of California, Riverside, CA 92521, USA*

† Electronic supplementary information (ESI) available. See DOI: 10.1039/c4cp02328e

defects which could be used as resonating sites in the resonator. Furthermore, removing or replacing lines of atoms creates phononic waveguides through which phonons can propagate. By engineering specific defects near these waveguides, the propagation of the phonons can also be controlled and manipulated leading to the realization of a phononic switch. Though it is possible to design such defect-based phononic components in the bulk materials, in this study, we focus on the realization of the phononic interconnect components on the surfaces of these materials.

In our study, we use molecular dynamics (MD) simulations, as implemented in the LAMMPS code[34] for our calculations of the partial phonon density of states (PPDOS), and the total density of states (TPDOS). We choose the Tersoff potential as our potential of choice.[35,36] This method has been used in our prior work on similar systems and tends to produce vibrational and structural properties, which were in good agreement with more rigorous ab initio calculations.[36] Though the initial frequency offsets in phononic band gap (PBG) edges and higher frequency phonons are up to 30%, further optimization and fitting led to the reduction in those offsets to less than 5%.[30] We validate our MD produced vibrational properties with those obtained from ab initio calculations[37] for smaller systems, and they are qualitatively and quantitatively in good agreement.

II. Computational methods

(a) Ab initio calculations

Ab initio calculations were performed using the generalized gradient approximation (GGA) employing the exchange–correlation functional of Perdew, Berke, and Ernzerhof (PBE)[37] expanding the wavefunction on plane-wave basis sets. We used standard Vanderbilt ultrasoft pseudopotentials.[38] The plane wave basis set cut-off is 240 eV. For the sampling of the Brillouin zone, we use a $6 \times 6 \times 1$ Monkhorst–Pack mesh. Tight convergence criteria have been imposed for the total (self-consistent) energy per atom at 2×10^{-5} eV per atom, while the threshold on the forces is set to 10^{-3} eV Å^{-1}. For the phonon DOS calculations, the dynamical matrix elements were calculated in the first Brillouin zone on a $6 \times 6 \times 1$ q-point mesh using a supercell of about 10 Å. A suitable Gaussian broadening of the dynamic matrix eigenvalues was used for the creation of the phonon DOS curves with a full width at half maximum of 3.3 cm^{-1}. The calculations have been performed using the electronic structure calculation package QUANTUM ESPRESSO.[39]

(b) Molecular dynamics simulations

Molecular dynamics (MD) simulations were performed with the LAMMPS code,[34] to study the vibrational properties of both the bulk and the surface of the SiC and GeSi crystals. The pair-wise interactions were computed with the Tersoff potentials for the C–C, C–Si, Si–Si, Si–Ge and Ge–Ge interactions.[35,36] All of the MD simulations are performed within the framework of the isothermal–isobaric ensemble (*NPT*), with a fixed number of atoms N, constant pressure P, constant temperature T, and a time step of 0.8 femtosecond (fs).

The temperature of the system was held constant at 300 K using the Nose–Hoover thermostat.[40,41] The Nose–Hoover thermostat allows for fluctuations of the temperature with a distribution close to the canonical distribution, thus probing the canonical ensemble quite accurately. The effective relaxation time τ affects the coupling with the internal heat bath. A long τ results in slower convergence to the canonical ensemble, while a short τ, can result in large, high-frequency fluctuation in the temperature. In our simulations, we used an effective relaxation time of 0.1 ps, which gives a good convergence and small fluctuations of the temperature close to the canonical distribution. The pressure of the system was maintained at 1 bar using the Nose–Hoover barostat, and a relaxation time of 1 ps.[34]

For our simulations, the base cell of choice was the primitive cell of the FCC Bravais lattice (triclinic) with a diatomic basis AB, where A is Si (Ge) and B is C (Si) for the cases of the 3C-SiC (3C-GeSi) crystals (see Fig. 1a). By replicating the base cell several times along the x, y and z directions, supercells with thousands of atoms were generated with their faces parallel to the $\langle 111 \rangle$ crystallographic plane. For bulk systems, the size of the structures was made equal to the size of the simulation box, as shown in Fig. 1b, and the barostat was set to relax the system in all directions. The $\langle 111 \rangle$ surface (see Fig. 1c) was constructed by replicating the base cell five times in the z-direction, and several times in the x- and y-directions. In order to avoid spurious interaction in the z-direction, a large enough vacuum gap was maintained above the supercell, so that the atoms in the top will not feel the interactions from the atoms in the bottom (due to the PBC along the z-axis), and thus behave as surface atoms. Systems with vacuum gaps ≥ 5 Å showed the exact same behavior as systems with very large vacuum gaps. Consequently, the structure becomes periodic along the x- and y-directions, and hence, the volume and pressure relaxes only along these directions. Note that, in order to avoid any unwanted surface effects related to the thickness of the structures, and to eliminate any thickness dependent frequency changes, as discussed in ref. 16 and 42, we tested the effect of thickness dependence. Increasing the thickness of GeSi from $\sim$6 to $\sim$16 Å leads to on average blue-shifts of 0.3 THz in the phonon DOS. However, increasing the thickness further leads to a negligible change ($\sim$0.05 THz) in the phonon spectra. Hence to minimize the required simulation time and computational resources, we have used five unit cells ($\sim$13 Å for SiC and $\sim$16 Å for GeSi) to model the structures with infinite thickness. This confirms that the examined surfaces should behave as the surfaces of the bulk materials in the range of THz frequencies.

The phonon density of states was calculated independently using two different methods. In the first method, the finite temperature phonon DOS was calculated by the Fourier transformation of the velocity time autocorrelation function (VACF),[30]

$$D(\omega) = \int_0^\infty \mathrm{d}\tau\, \mathrm{e}^{i\omega\tau} \frac{1}{N} \sum_{i=1}^{N} \frac{1}{t_{\max}} \sum_{t_0=1}^{t_{\max}} \vec{v}_i(t_0) \cdot \vec{v}_i(t_0 + \tau) \qquad (1)$$

where $\vec{v}_i$ is the velocity of the ith atom, N is the number of the selected atoms, and t_0 is the initial time step. For the total

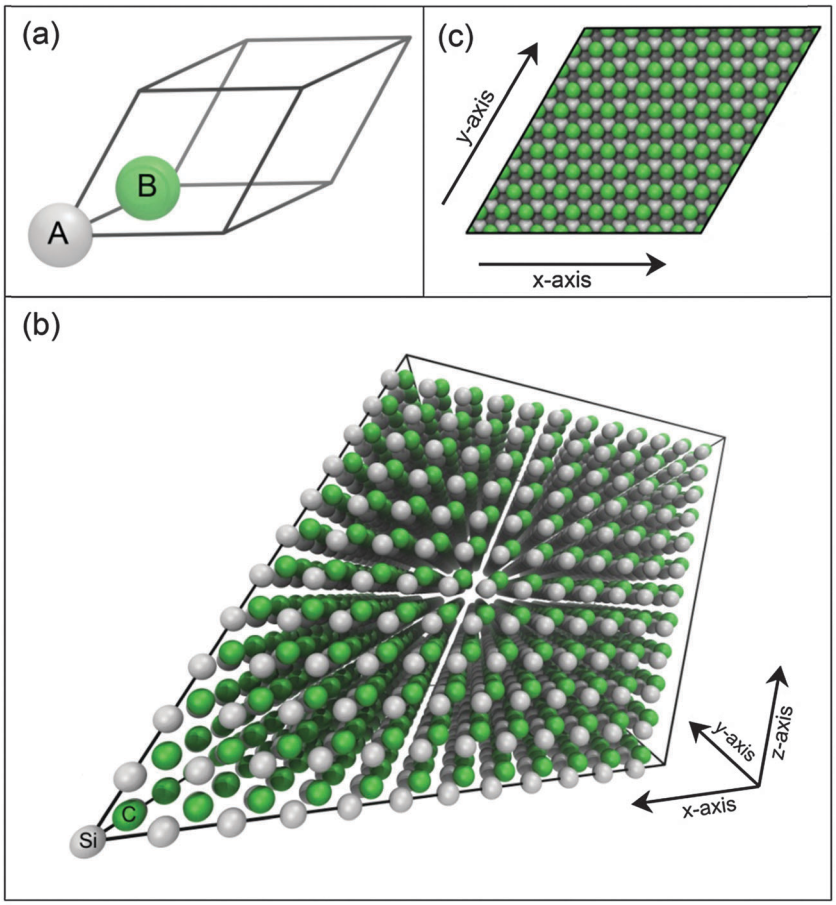

Fig. 1 (a) The primitive cell (triclinic) of the FCC lattice with a diatomic basis AB, where A is Si (Ge) and B is C (Si). (b) The bulk structure of 3C-SiC, generated by 12 replications of the primitive cell (a), in the *x*, *y* and *z* directions. (c) The ⟨111⟩ surface of SiC. Note that the atoms in the background (dark grey) are also Si atoms.

phonon density of states (TPDOS), the structures were allowed to relax for 160 ps (2×10^5 time steps), and then the velocities of all the atoms in the system (N_{system}) were captured every 3.2 fs (4 time steps), for a total time of 13.1 ps (2^{14} time steps). To evaluate the TPDOS, these captured velocities were input into eqn (1). For the partial phonon density of states (PPDOS) calculation, the velocities of specified groups of atoms ($1 < N < N_{\text{system}}$), or single atoms ($N = 1$) were captured instead and then used in eqn (1). In order to improve the accuracy of the PPDOS and avoid any statistical sampling issue, the size of the statistical sample is increased by capturing the velocities of the selected atoms in 10 independent iterations instead of one, and then averaging the calculated velocity autocorrelation functions. In order to check the consistency of the observed results and avoid any relaxation time dependent results, we also performed test simulations at longer relaxation times, and found no direct correlation between the relaxation time and quality of the phonon spectra.

In the second method, we used the FixPhonon module available in the LAMMPS distribution.[34,43,44] In this module, prior to analyzing the lattice vibrations of the given system, the system was equilibrated at room temperature by calibrating at various time scales. The instantaneous positions of atoms in the equilibrated system were transformed into reciprocal space to obtain the Green's function. After a certain number of measurements, the "time" average of the Green's function was evaluated, and, for a long enough simulation, the time average was equivalent to an "ensemble" average. The force constant matrices were then deduced, and the dynamical matrices were constructed from them. During the dynamic matrix calculation, at a given temperature and pressure, the systems were equilibrated for 10^6 MD steps, and then the time average of the phonon frequencies was calculated for 6×10^6 MD steps. Using the eigenvalues of these dynamical matrices, the TPDOS and PPDOS were computed. In order to observe smoother DOS, a dense wave vector is recommended,[43] thus in our simulations we replicated our supercell several times and then used an even denser wave vector in the post-processing stage. This requirement increases the size of the supercell from 20–50 atoms to approximately 5×10^3 to 10^4 atoms.

For all the structures in this study, both the VACF and FixPhonon methods produced qualitatively and quantitatively similar vibrational properties. Though the VACF method is free from any requirement of supercell replication and hence, intensive computing resources, the phonon spectra were noisier than the one produced by the FixPhonon method. Irrespective of

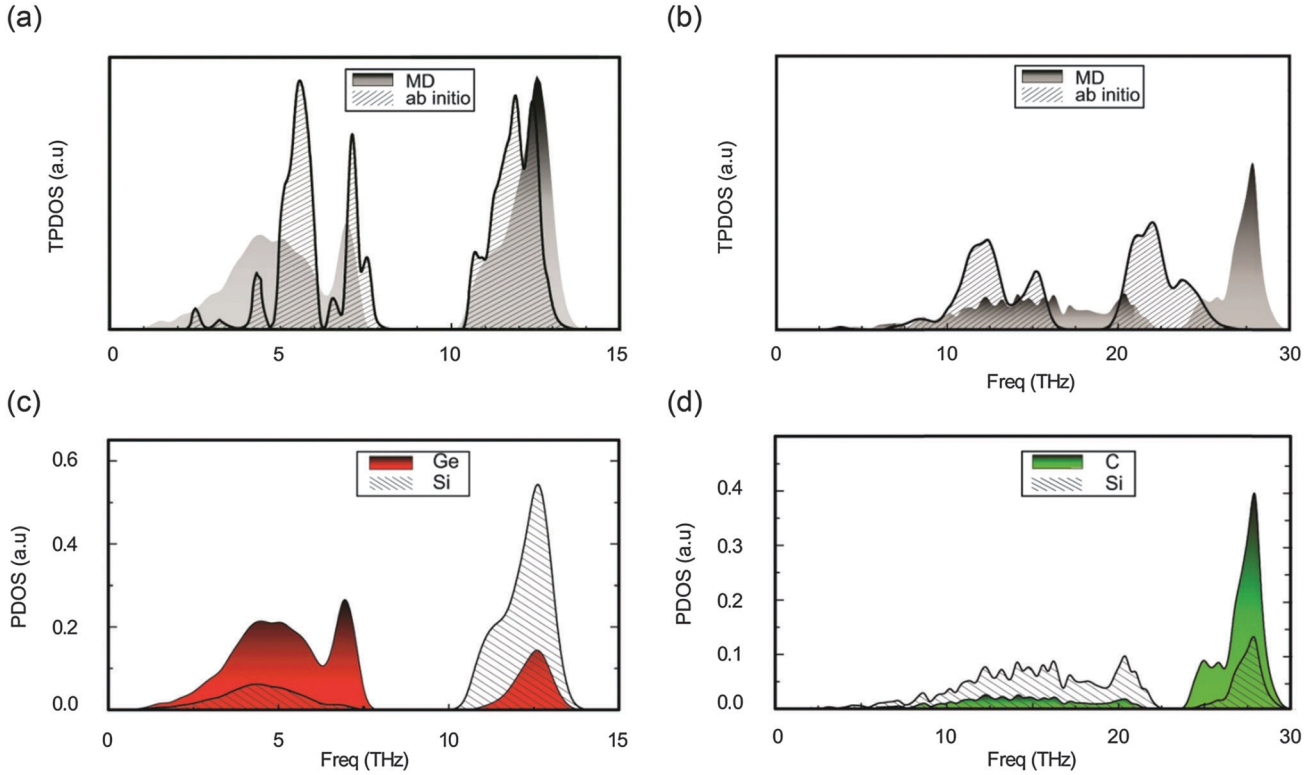

Fig. 2 Phonon density of states of the bulk GeSi (a) and SiC (b) systems. The grey curves represent MD simulation results, the solid black curve with the hatched fill pattern represents ab initio results, and (c and d) the partial phonon density of states (PPDOS) of the bulk GeSi (c) and SiC (d) from MD simulations. The PPDOS for the C, Si and Ge atoms are represented by green, hatchet fill pattern and red curves, respectively.

the higher computational cost, throughout this study, we present the FixPhonon method since the results were of higher quality, though all of our results were verified with both methods.

III. Results and discussion

(a) Phonon density of states of the bulk

Molecular dynamics (MD) is an empirical atomistic model, and its empirical parameters should be calibrated and verified either against available experimental data or first principle data to verify the accuracy of the model. Since there is a lack of the experimental data on our system, we compare our bulk GeSi and SiC vibrational properties with those obtained from first principle (ab initio) calculations. The solid black curve with the hatched fill pattern in Fig. 2a shows the ab initio TPDOS for GeSi with a phononic band gap (PBG) between 8.3 and 10.7 THz and a maximum frequency at approximately 13.5 THz. The solid grey region shows the MD TPDOS with a PBG between 7.8 and 10.3 THz and a maximum frequency at 13.8 THz. The TPDOS of the bulk SiC and GeSi from the VACF method are included in ESI,† Fig. S1.

The ab initio calculated PBG for bulk SiC (solid curve with hatched fill in Fig. 2b) is between 16.7 and 19.2 THz, and the maximum frequency phonon is at around 27 THz. The MD simulations (Fig. 2b, grey region) give a PBG between 22.3 and 23.9 THz and a maximum phonon frequency at 29 THz. The PBG resulting from the MD simulation is shifted by 20–30% towards higher frequencies with a width 36% smaller than the result from the ab initio calculation.

It is clear that the interatomic potential[35,36] does not describe the lattice dynamics and inter-layer coupling of SiC as accurately as for GeSi. However, as will become clear from the rest of our results, the trends are the same for both GeSi and SiC indicating the validity of the calculations.

Though the ab initio method for the SiC system produces better results, it is computationally expensive, as compared to the MD method. In addition, most of our examined structures have several thousand atoms, and hence, analyzing the vibrational properties using ab initio methods is not feasible, mainly due to the computational time and memory constraints. Fig. 2c and d illustrate the partial density of states (PPDOS) of bulk GeSi and bulk SiC, respectively, calculated using the MD method.

(b) The ⟨111⟩ surface of the 3C-GeSi and 3C-SiC

Fig. 1c illustrates the atomistic view of the ⟨111⟩ surface of 3C-SiC, similar to the ⟨111⟩ surface of 3C-GeSi. The constructed surfaces have two possible configurations based on the type of atoms covering the surface. In the first configuration, the surface is covered with the lighter atoms *i.e.* Si-face (C-face) for the cases of GeSi (SiC), as shown in Fig. 1c. In the second configuration, the heavier atoms are on the surface Ge-face (Si-face) for GeSi (SiC).

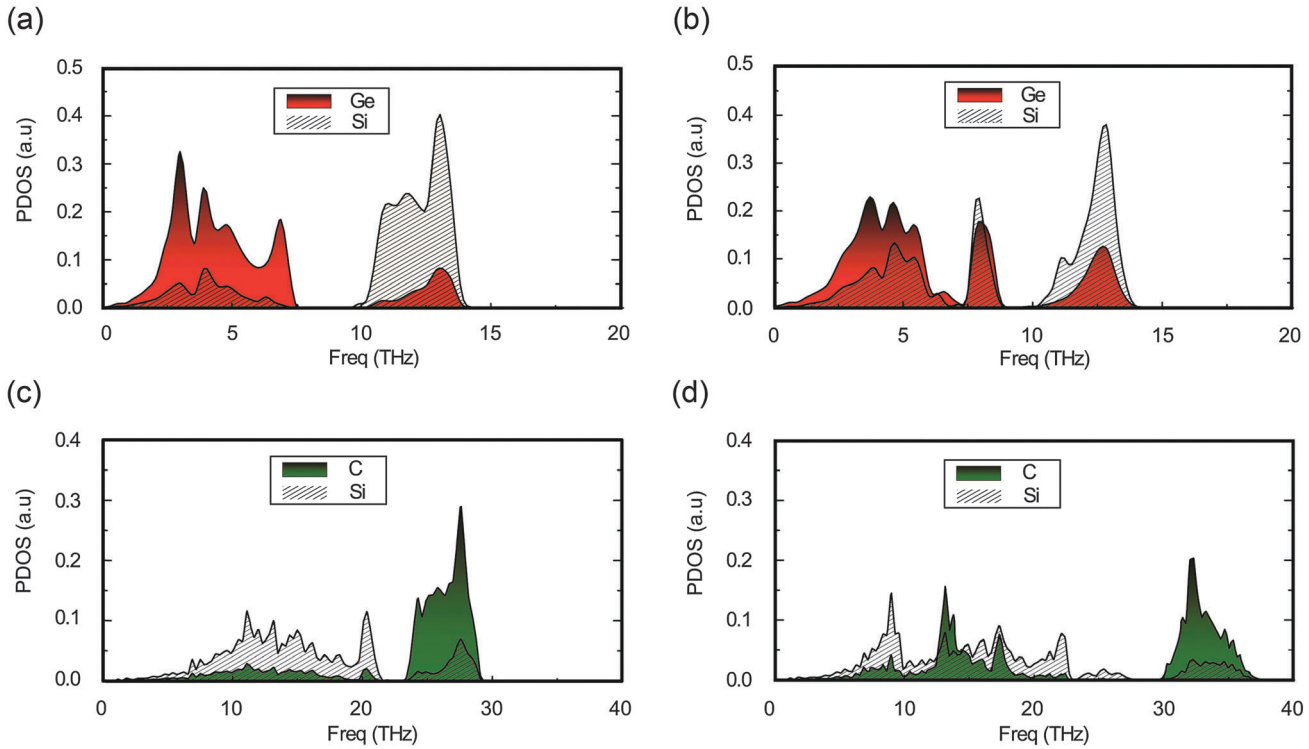

Fig. 3 The PPDOS of the ⟨111⟩ surfaces of 3C-GeSi and 3C-SiC. The PPDOS of the (a) Ge-face, (b) Si-face of GeSi. The PPDOS of the (c) Si-face, (d) C-face of SiC. For all the cases, the green, hatchet fill pattern and red curves correspond to the C, Si and Ge atoms respectively.

The PPDOS of the Ge-face surface of GeSi in (Fig. 3a) is qualitatively similar to the bulk GeSi (Fig. 2c), with a slight blue-shift (~0.5 THz) in the maximum phonon frequency. In contrast, the PPDOS of the Si-face (Fig. 3b) shows a new surface state inside the PBG around 8 THz. This feature is also observed in the case of SiC. When the heavy atom (Si) is on the surface (Si-face), the PPDOS (Fig. 3c) is similar to that of bulk SiC (Fig. 2b) with a slight redshift of the PBG by 0.5 THz. Interestingly the PPDOS of the C-terminated surface shows a maximum frequency peak at about 30 to 37 THz, well above the highest frequency phonon of the bulk SiC, while the PBG is significantly reduced (~23 to 23.5 THz), as illustrated in Fig. 3d.

The C atoms in 3C-SiC crystals with randomly induced substitutional defects have a total of five possible configurations, since they neighbor with zero to four C atoms (and consequently with four to zero Si atoms). When the C atoms neighbor with four other C atoms by forming the diamond configuration, the observed maximum phonon frequencies are 33 THz. In the case where the C atoms neighbor with four Si atoms (SiC configuration), the PPDOS has maximum phonon frequencies of 29 THz (Fig. 2d). This is mainly due to the damping of the higher frequency vibration of the lighter C atoms when surrounded by the heavier Si atoms. This also applies to the atoms on the surface. On the C terminated surface of SiC, the C atoms neighbor with just three Si atoms instead of four (the configuration in the bulk), and thus, the phonon branches of these atoms tend to shift in higher frequencies. Similar suppression and release of the phonon branches is also observed in the GeSi system.

It is important to point out that these surface states appear either inside the PBG, or above the maximum frequency phonon of the bulk. These states, if excited, will not leak in the bulk region but instead will propagate on the surface. In the rest of this study, these surface states will be used for designing the resonators (isolated defects), the waveguides (lines with defects) and the switches (defects in the waveguides), which enhance the propagation of the phonons.

(c) Resonators

The resonators can be created on the surface either by introducing single substitutional or vacancy defects. In the first type of resonator, a substitutional defect was introduced by exchanging one Ge atom with one Si atom in the Ge-face of the GeSi surface (see the inset in Fig. 4a). The introduction of the substitutional defect gives rise to two new phonon states: (a) one around 8 THz (inside the PBG of both the bulk GeSi and the ⟨111⟩ Ge-face) and (b) another around 16 THz (above the highest frequency phonon of both the bulk GeSi and the Ge-face surface). These states are well localized around the defect. Substitutional defects in the ⟨111⟩ Si-face of the SiC surface exhibit similar behavior. The PPDOS of the replaced atom (Si ↔ C), as shown in (Fig. 4b) features a PBG between 22 and 23 THz. The observed frequency maxima is around 38 THz (above the maximum phonon frequency of both the bulk SiC and the ⟨111⟩ Si-surface of the SiC).

The second type of resonator was designed by introducing a single vacancy defect in the Ge-face of the GeSi surface (inset in Fig. 4c). The PPDOS for the neighboring Si atom (marked with an arrow in the inset of Fig. 4c) exhibits a peak at around 8 THz.

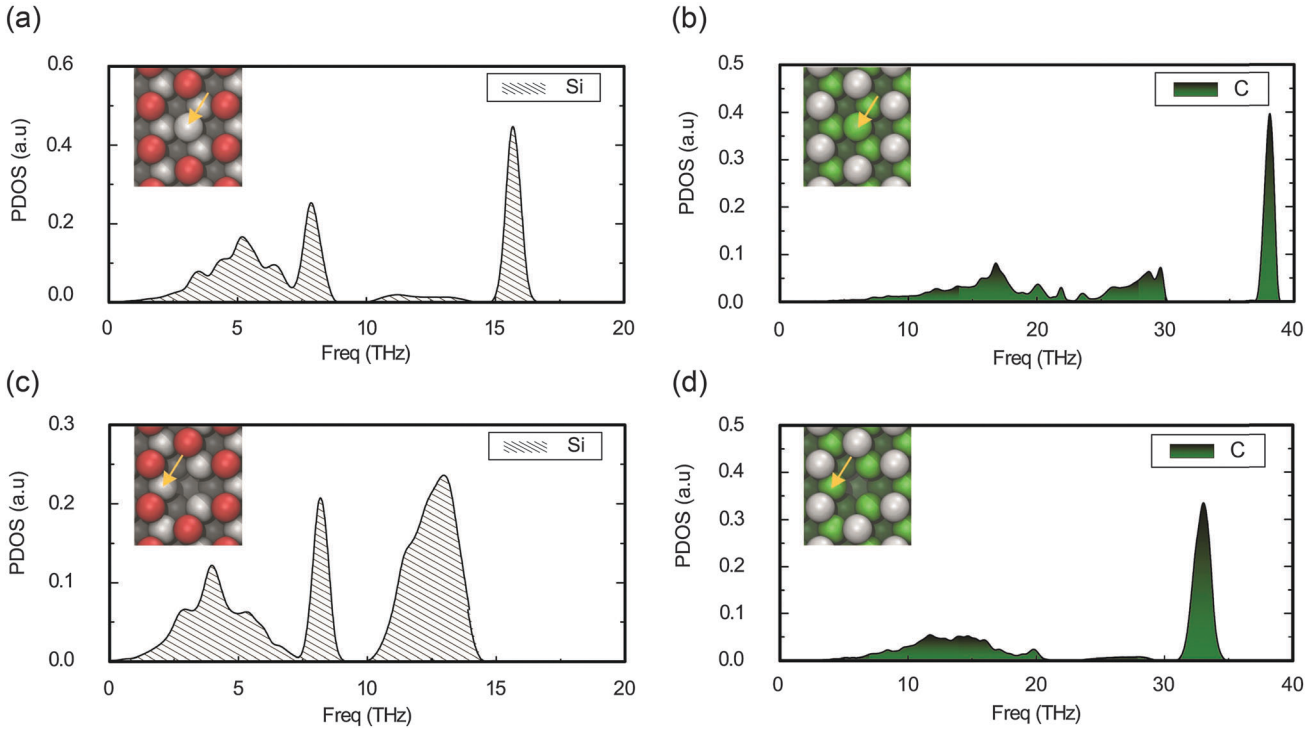

Fig. 4 PPDOS of isolated substitutional and vacancy defects in the ⟨111⟩ surface of 3C-GeSi and 3C-SiC. The PPDOS of the Ge-face of GeSi surface with (a) a substitutional defect and (c) a single vacancy defect. The PPDOS of the Si-face of the SiC surface with (b) a substitutional defect and (d) a single vacancy defect. The inset in each figure illustrates the configurations for the corresponding case. For all the cases, the PPDOS corresponds to the atoms marked with the yellow arrows. The green, grey and red colors correspond to the C, Si and Ge atoms, respectively.

This peak is inside the PBG of both the bulk GeSi (refer to Fig. 2c) and the ⟨111⟩ Ge terminated surface (refer to Fig. 3a). Albeit the steeper maximum peak, the overall PPDOS feature is similar to the case of the Si-face of the GeSi surface, as shown in Fig. 3b, because, in both cases, the examined Si atoms share the same local configuration (both of them neighbor with three Ge atoms). In the case of the Si-face of SiC, the PPDOS of the C atom located near the vacancy (marked with an arrow in the inset of Fig. 4d) exhibits a well-defined peak at around 33 THz. The peak is well above the maxima in the phonon frequencies of both the bulk SiC (refer to Fig. 2d) and the ⟨111⟩ Si-surfaced SiC (refer to Fig. 3c). Similar to the substitutional induced defect states, the phonons corresponding to vacancy defects are well localized around the defects.

(d) Waveguides

Similar to the resonators, we designed waveguides by creating lines with substitutional or vacancy defects in the ⟨111⟩ surfaces of GeSi and SiC. Initially, a single line of Ge atoms was replaced with Si atoms (see Fig. 5a) in the Ge-face of GeSi. The PPDOS of the Si atoms in the line features two well defined peaks at around 8 and 16 THz, as illustrated in Fig. 5d (grey curve). The PPDOS of this waveguide is similar to the PPDOS of the Si resonator, as shown in Fig. 4a. Since these states are absent in the phonon DOS of the bulk and the Ge-face, they will be able to propagate only along the line of Si defects on the Ge-surface of GeSi. As the width of the waveguide increases to two and three Si atoms, as shown in Fig. 5b and c, the highest frequency phonons

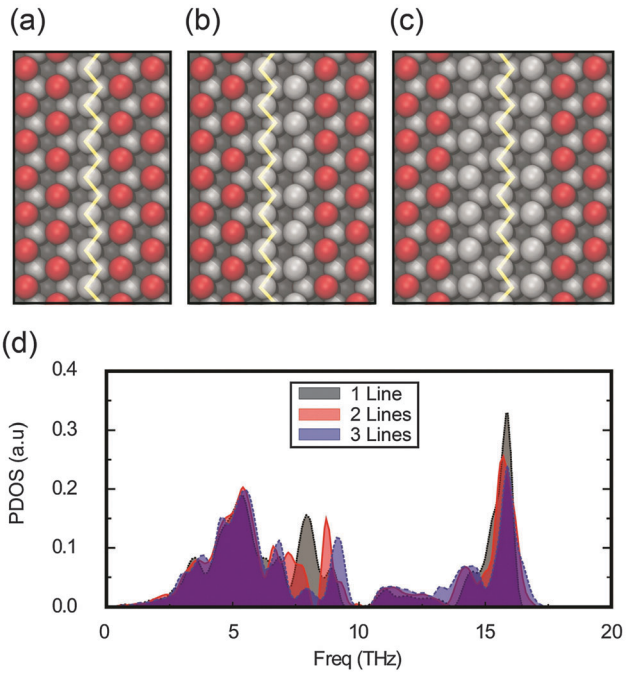

Fig. 5 Atomistic representations of Ge-terminated surfaces of GeSi, with (a) one line, (b) two neighboring lines, and (c) three neighboring lines, with substitutional defects. The red and grey atoms correspond to Ge and Si respectively. (d) The PPDOS of the atoms in the waveguides for one (grey), two (red), and three (blue) neighboring lines with vacancy defects.

appear at around 17 and 17.2 THz, respectively, as illustrated in Fig. 5d (red and blue curves). For the two and three atom widths, the lowest bound of the PBG shifts to higher frequencies at around 9.7 and 9.9 THz, respectively, leading to the reduction of the PBG gaps, while the higher edges remain unaltered. For four and more atom widths of the waveguide, the PBG width of the PPDOS remains constant. Note that these states were also observed in the PPDOS of the neighboring Si atoms, just below the defect line. Similar results were also obtained for the waveguides with the substitutional defects in the Si-face of SiC.

Introducing substitutional defects using C atoms along a single line completely fills the PBGs of the bulk SiC and the Si-face SiC. Consequently, a few new states emerge in between 33.5 and 40 THz, well above the phonon frequency maxima of the bulk SiC, and hence, a new PBG appears in between 30.5 and 33.5 THz. By increasing the width of the waveguide to two C atoms, the newly formed PBG of the single line is partially filled with the new states. Further increment of the line-width leads to the filling of the gap and the disappearance of the PBG.

Besides substitutional defects, waveguides can also be designed by removing lines of atoms (vacancy defects) from the surface. Initially a waveguide with a line with vacancy defects in the Ge-face of the GeSi is designed, as shown in Fig. 6a. Hereafter, we call this type of waveguides as TYPE-S. The PPDOS of either a Si atom just below the defect line or a Ge atom next to the defect line shows a peak at around 8.2 THz as in Fig. 6b. Unlike the waveguide from substitutional defects, it does not exhibit any additional mode above the maximum phonon frequencies of either the bulk GeSi, or the ⟨111⟩ Ge-surface of GeSi.

Removing two or more neighboring lines of Ge atoms from the ⟨111⟩ Ge-face of the GeSi makes the Si atoms just below those defect lines unstable, and they detach from the rest of the structure at room temperature. This is expected because these atoms, after losing three of their neighbors, become unstable due to the reduction of their bonding energies. Beside this case, all the other cases studied above were stable. Another possible type of stable waveguide (TYPE-D) can be created by removing two lines of Ge atoms on each side of a Ge line, as shown in Fig. 6c. The PPDOS of this wave guide, as illustrated in Fig. 6d, displays similar behavior to that of the single line vacancies in the Ge-face of GeSi (Fig. 6b), with a peak at 7.8 THz. However, it has an additional narrow peak at around 8.5 THz.

In addition to the linear waveguides, controlled addition or removal of defects in the surface could lead to the realization of a phononic component that could not only modulate the phonons but also, split and redirect the propagation into different directions. This phononic waveguide, which could modulate phonons, is an analogous component to the electrical or optical waveguide.[20] Fig. 7 illustrates such structures made from substitutional and vacancy defects. The top structure (dotted black circles in Fig. 7a and b) bends the propagation path of the propagating phonons, and we call this phononic

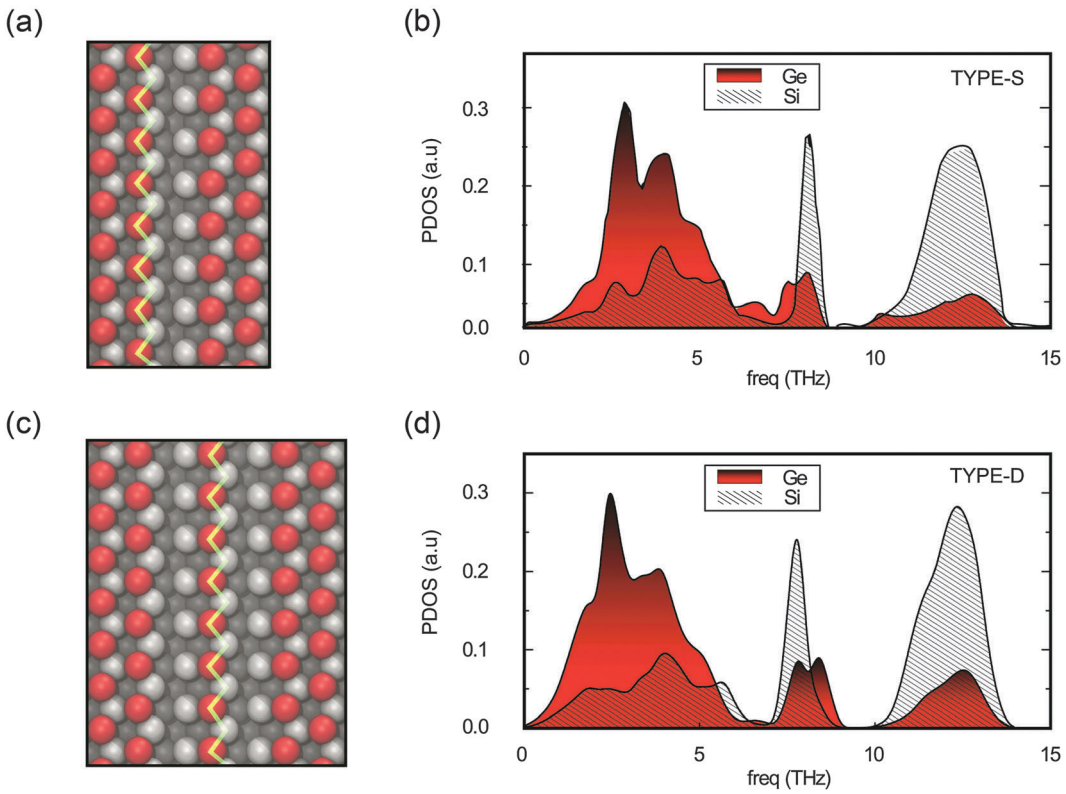

Fig. 6 Vacancy waveguides in the Ge-face of the GeSi surface, (a) TYPE-S and (c) TYPE-D. PPDOS for the Si and Ge atoms in the TYPE-S (b) and TYPE-D (d) waveguides. The red and grey colors correspond to Ge and Si, respectively.

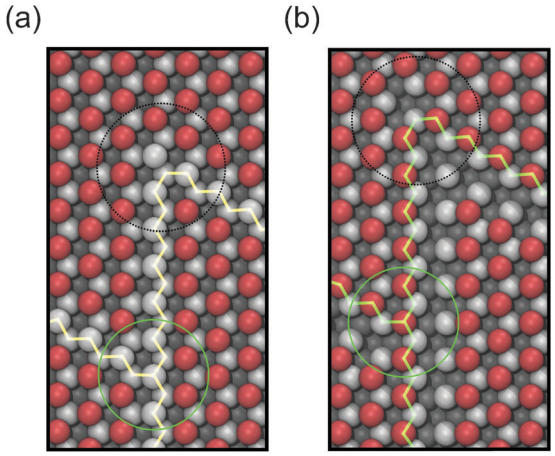

Fig. 7 Illustration of the phonon propagation in complex phononic waveguides, which splits phonons into two paths (phonon-splitters, green circles), or modulates the direction (phonon-benders, dotted black circles). Complex phononic waveguides designed with (a) substitutional defects, and (b) with vacancy defects, in the Ge-face of GeSi. The grey and red atoms are Si and Ge, respectively. The phonon propagation paths are illustrated using the zigzag lines.

component a phonon-bender. Similarly, the bottom structure (green-dotted circles in Fig. 7a and b) splits the propagating phonons, and this component is known as the phonon-splitter. When the propagating phonons reach the phonon-bender they will change direction (120° turn). Similarly, when the propagated phonons reach the phonon-splitter, they will split into two different directions. Using this method of inducing the substitutional defects, one can design phonon-splitters that could split the transmitting phonons in many different directions. Note that a Ge atom is missing from the top of the waveguide with the vacancy defects (Fig. 7b). This intentional removal of Ge atom is needed because the Si atoms in the waveguide are required to neighbor with only three Ge atoms to sustain the resonant peak at 8 THz frequency.

(e) Switches

By inducing defects at the waveguides, one can also enhance the propagation of the phonons, and design phononic switches, analogous to electronic and optical switches. Here, we have designed the phononic switch by placing adatoms in the middle of the vacancy waveguide, as shown in Fig. 8a. The PPDOS of a Si atom (marked with the black arrow) that neighbors to a Ge adatom (marked with the yellow arrow) placed in the middle of a vacancy waveguide, at the Ge-terminated surface, is shown in Fig. 8b. In this structure, there is no resonant peak in the frequency region between 7 and 10 THz, indicating the blocking of the guiding mode at around 8 THz, which was present in the simple waveguide case (refer to Fig. 6b). Using this property, one can envision a phononic component having a ⟨111⟩ Ge-terminated surface of GeSi with a vacancy waveguide and a scanning tunneling microscope (STM) tip consisting of Ge atoms that can be tuned in or out of the waveguide. The novelty of these types of components would be their ability to allow or block the propagation of phonons along the waveguide at the atomic-level.

Besides adatom defects, we also investigated the possibility of using other kinds of defects within the waveguide. Since the phonons can only be transmitted through the atoms that are located either below or next to the waveguide, introducing a vacancy defect in the waveguide blocks the propagation of the phonons in its entirety. On the other hand, substitutional defects within the waveguide do not seem to block the phonon transmission. We also observed that exchanging a Si atom with a Ge atom either within (Fig. 9a) or near (Fig. 9c) the waveguide does not affect the resonant peak at ~8 THz, thus the phonons are allowed to propagate without any scattering. This confirms that introduction of random substitutional defects, through natural diffusion, should not block the transmission of the phonons, and hence, the waveguide should continue to be functional.

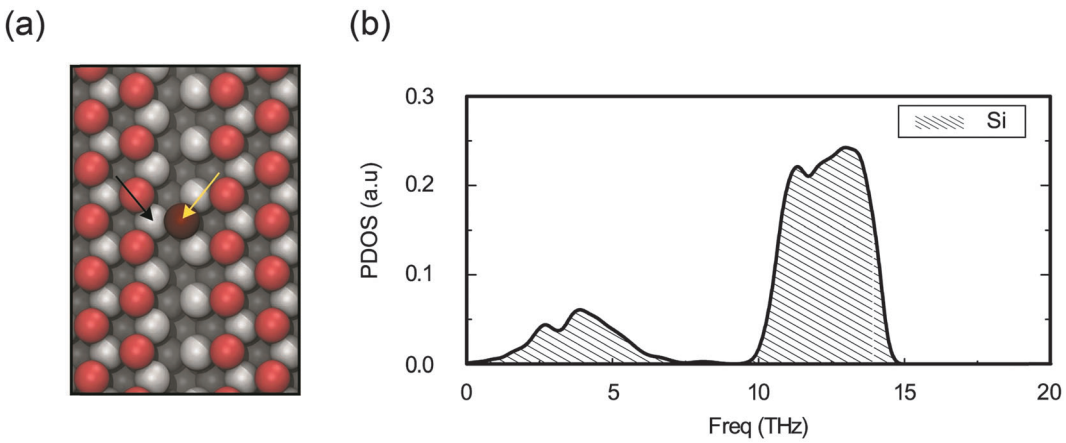

Fig. 8 (a) Atomistic representations of a phononic switch designed by adding a Ge adatom (dark red atom marked with a yellow arrow) on the TYPE-S waveguide in the Ge-face of GeSi. (b) The PPDOS of the Si atom (marked with a black arrow in (a)) that neighbors to the Ge adatom (switch). Note that the resonant peak at 8 THz is suppressed.

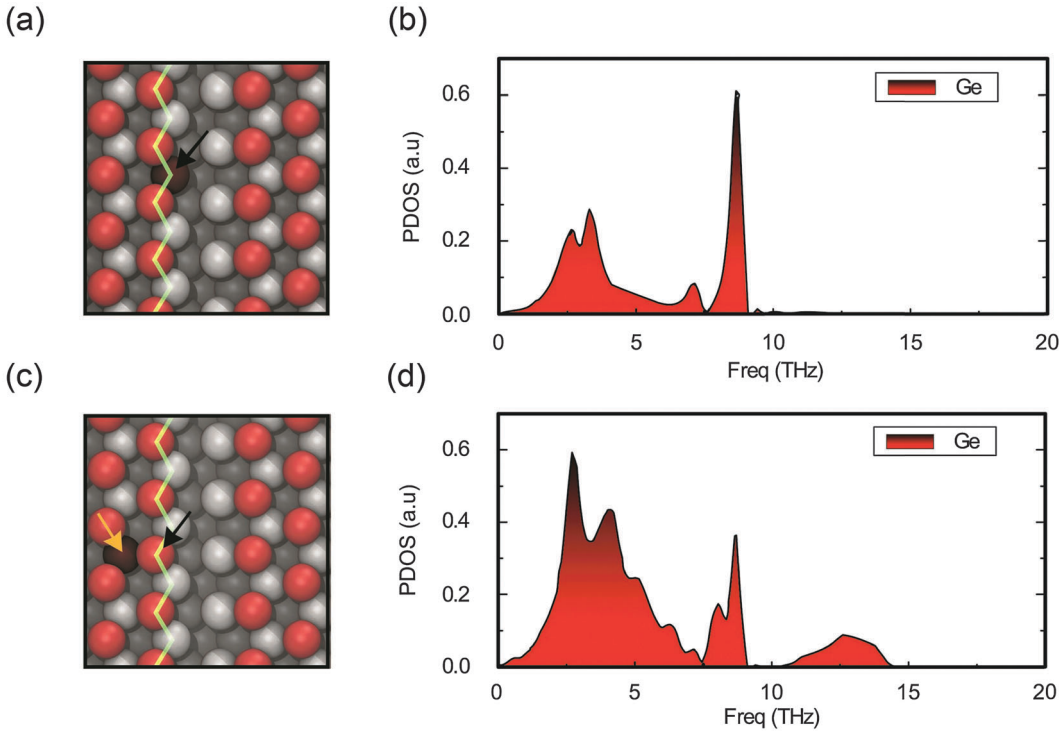

Fig. 9 Substitutional defects (dark red) inside (a) and near (c) the TYPE-S vacancy waveguides in the Ge-face of GeSi. The yellow arrow at (c) points to the substitutional defect. (b) The PPDOS of the Ge atom marked with a black arrow in the configuration of (a). (d) The PPDOS of the Ge atom marked with a black arrow in the configuration of (c). The red and white atoms represent the Ge and Si atoms, respectively, while the dark red atoms represent the substitutional defects (Si ↔ Ge).

IV. Conclusions

Phononic interconnects on the ⟨111⟩ surface of the 3C-SiC and 3C-GeSi system were conceptualized and designed using defect engineering techniques with the framework of atomistic molecular dynamics (MD) method. The existence of phononic band gaps within the phonon spectrum of the bulk 3C-SiC and 3C-GeSi was confirmed by both the ab initio and MD simulations with semi-empirical potentials. The agreement between the two methods was good for the case of 3C-GeSi and moderate for the 3C-SiC case, mainly due to the inaccuracies in the Si–C interaction parameters in the Tersoff's potential. The PPDOS on the ⟨111⟩ surface of these systems reveals the possibility of generating the new surface states within the phononic band gap (especially for the case where the lighter atoms are in the surface). These surface states, which are decoupled from the bulk states, are used to design phononic interconnects, such as resonators (isolated defects), waveguides (lines with defects), and switches (adatoms within the waveguide). In conjunction with electronic and/or photonic interconnects, these proposed phononic interconnects could be used in the current and future devices, while expanding overall computing and memory capabilities.

Although the present study demonstrates the possibility of realizing phononic interconnects in the atomic scale, there are several important issues that need to be addressed before they can be integrated in the current and future technologies. Some of these issues are excitation frequency, coupling losses, propagation losses, optimum materials and structures, and surface passivation.

Acknowledgements

This work is supported in part by the National Science Foundation (NSF) Grant No: 1307671, FAME, one of six centers of STARnet, a SRC program sponsored by MARCO and DARPA, and a U.S. Dept. of Education GAANN Fellowship (MRN). This work used the computational resources at Purdue University and University of Patras.

References

1 A. A. Balandin and D. L. Nika, *Mater. Today*, 2012, **15**, 266–275.
2 M. Maldovan, *Nature*, 2013, **503**, 209–217.
3 M. M. Sigalas and E. N. Economou, *J. Sound Vibr.*, 1992, **158**, 377–382.
4 M. S. Kushwaha, P. Halevi, L. Dobrzynski and B. Djafari-Rouhani, *Phys. Rev. Lett.*, 1993, **71**, 2022–2025.
5 C. W. Chang, D. Okawa, A. Majumdar and A. Zettl, *Science*, 2006, **314**, 1121–1124.
6 D. Segal, *Phys. Rev. Lett.*, 2008, **100**, 105901.
7 N. Boechler, G. Theocharis and C. Daraio, *Nat. Mater.*, 2011, **10**, 665–668.
8 S. R. Sklan and J. C. Grossman, arXiv:1401.6537v1.

9 L. Wang and B. Li, *Phys. Rev. Lett.*, 2008, **101**, 267203.
10 J. Khan, C. M. Nolen, D. Teweldebrhan, D. Wickramaratne, R. K. Lake and A. A. Balandin, *Appl. Phys. Lett.*, 2012, **100**, 043109.
11 P. Goli, K. Khan, D. Wickramaratne, R. K. Lake and A. A. Balandin, *Nano Lett.*, 2012, **12**, 5941–5945.
12 T. Ouyang, Y. Chen, Y. Xie, G. M. Stocks and J. Zhong, *Appl. Phys. Lett.*, 2011, **99**, 233101.
13 A. A. Balandin, *Nat. Mater.*, 2011, **10**, 569–581.
14 P. Goli, S. Legedza, A. Dhar, R. Salgado, J. Renteria and A. A. Balandin, *J. Power Sources*, 2014, **248**, 37–43.
15 P. E. Hopkins, C. M. Reinke, M. F. Su, R. H. Olsson, E. A. Shaner, Z. C. Leseman, J. R. Serrano, L. M. Phinney and I. El-Kady, *Nano Lett.*, 2011, **11**, 107–112.
16 J. Cuffe, E. Chávez, A. Shchepetov, P. O. Chapuis, E. H. El Boudouti, F. Alzina, T. Kehoe, J. Gomis-Bresco, D. Dudek, Y. Pennec, B. Djafari-Rouhani, M. Prunnila, J. Ahopelto and C. M. Sotomayor Torres, *Nano Lett.*, 2012, **12**, 3569–3573.
17 M. Maldovan, *Phys. Rev. Lett.*, 2013, **110**, 025902.
18 B. L. Davis and M. I. Hussein, *Phys. Rev. Lett.*, 2014, **112**, 055505.
19 M. J. R. Heck, H.-W. Chen, A. W. Fang, B. R. Koch, D. Liang, H. Park, M. N. Sysak and J. E. Bowers, *IEEE J. Sel. Top. Quantum Electron.*, 2011, **17**, 333–346.
20 P. Chaisakul, D. Marris-Morini, J. Frigerio, D. Chrastina, M.-S. Rouifed, S. Cecchi, P. Crozat, G. Isella and L. Vivien, *Nat. Photonics*, 2014, **8**, 482–488.
21 S. Dakshinamurthy, N. R. Quick and A. Kar, *J. Phys. D: Appl. Phys.*, 2007, **40**, 353.
22 P. Ščajev, M. Kato and K. Jarašiūnas, *J. Phys. D: Appl. Phys.*, 2007, **44**, 362402.
23 L. Huet, M. Ammar, E. Morvan, N. Sarazin, J.-P. Pocholle, J. Reichel, C. Guerlin and S. Schwartz, *Appl. Phys. Lett.*, 2012, **100**, 121114.
24 H. Kraus, V. A. Soltamov, D. Riedel, S. Väth, F. Fuchs, A. Sperlich, P. G. Baranov, V. Dyakonov and G. V. Astakhov, *Nat. Phys.*, 2014, **10**, 157–162.
25 S. Castelletto, B. C. Johnson, V. Ivády, N. Stavrias, T. Umeda, A. Gali and T. Ohshima, *Nat. Mater.*, 2013, **13**, 151–156.
26 Z. Zhong, W. Schwinger, F. Schäffler, G. Bauer, G. Vastola, F. Montalenti and L. Miglio, *Phys. Rev. Lett.*, 2007, **98**, 176102.
27 S. M. George, *Chem. Rev.*, 2010, **110**, 111–131.
28 Z. Zhong, H. Gong, Y. Ma, Y. Fan and Z. Jiang, *Nanoscale Res. Lett.*, 2011, **6**, 322.
29 Y. Luo, X. Zheng, G. Li, I. Shubin, H. Thacker, J. Yao, J.-H. Lee, D. Feng, J. Fong, C.-C. Kung, S. Liao, R. Shafiiha, M. Asghari, K. Raj, A. V. Krishnamoorthy and J. E. Cunningham, *Micromachines*, 2012, **3**, 345–363.
30 A. Sgouros, M. M. Sigalas, G. Kalosakas, K. Papagelis and N. I. Papanicolaou, *J. Appl. Phys.*, 2012, **112**, 094307.
31 M. M. Sigalas and E. N. koukaras, *Appl. Phys. Lett.*, 2012, **100**, 203109.
32 M. Fuechsle, J. A. Miwa, S. Mahapatra, H. Ryu, S. Lee, O. Warschkow, L. C. L. Hollenberg, G. Klimeck and M. Y. Simmons, *Nat. Nanotechnol.*, 2012, **7**, 242–246.
33 B. Weber, S. Mahapatra, H. Ryu, S. Lee, A. Fuhrer, T. C. G. Reusch, D. L. Thompson, W. C. T. Lee, G. Klimeck, L. C. L. Hollenberg and M. Y. Simmons, *Science*, 2012, **355**, 64–67.
34 S. Plimpton, *J. Comput. Phys.*, 1995, **117**, 1–19.
35 J. Tersoff, *Phys. Rev. B: Condens. Matter Mater. Phys.*, 1998, **37**, 6991.
36 J. Tersoff, *Phys. Rev. B: Condens. Matter Mater. Phys.*, 1989, **39**, 5566.
37 J. P. Perdew, K. Burke and M. Ernzerhof, *Phys. Rev. Lett.*, 1996, **77**, 3865–3868.
38 D. Vanderbilt, *Phys. Rev. B: Condens. Matter Mater. Phys.*, 1990, **41**, 7892.
39 P. Giannozzi, S. Baroni, N. Bonini, M. Calandra, R. Car, C. Cavazzoni, D. Ceresoli, G. L. Chiarotti, M. Cococcioni, I. Dabo, A. Dal Corso, S. Fabris, G. Fratesi, S. de Gironcoli, R. Gebauer, U. Gerstmann, C. Gougoussis, A. Kokalj, M. Lazzeri, L. Martin-Samos, N. Marzari, F. Mauri, R. Mazzarello, S. Paolini, A. Pasquarello, L. Paulatto, C. Sbraccia, S. Scandolo, G. Sclauzero, A. P. Seitsonen, A. Smogunov, P. Umari and R. M. Wentzcovitch, *J. Phys.: Condens. Matter*, 2009, **21**, 395502.
40 S. Nose, *J. Chem. Phys.*, 1984, **81**, 511–519.
41 W. G. Hoover, *Phys. Rev. A: At., Mol., Opt. Phys.*, 1985, **31**, 1695–1697.
42 G. Gopalakrishnan, M. V. Holt, K. M. McElhinny, J. W. Spalenka, D. A. Czaplewski, T. U. Schülli and P. G. Evans, *Phys. Rev. Lett.*, 2013, **110**, 205503.
43 L. T. Kong, *Comput. Phys. Commun.*, 2011, **182**, 2201–2207.
44 L. T. Kong and L. J. Lewis, *Phys. Rev. B: Condens. Matter Mater. Phys.*, 2008, **77**, 165422.

